Effect of Annealing on the Microstructure, Texture and Tensile Deformation Properties of Cu–3 wt%Ag–0.5 wt%Zr Thin Sheets Rolled at Room and Cryogenic Temperature

Peng Zhang[1] · Han Wang[1] · ShengJie Yao[1] · ChuanJie Wang[1] · Qiang Zhu[1] · Gang Chen[1]

Abstract

The Cu–3 wt%Ag–0.5 wt%Zr are rolled with the same reduction process at room (RT) and cryogenic (CT) temperature, respectively. The electron backscatter diffraction and transmission electron microscope are used to analyze and compare the evolutions of material microstructure and texture. The results show that the stability of as-rolled CT sheets is different from that of the RT samples, which can be verified by the lower temperature for the occurrence of recrystallization and Ag-base particles precipitation. Besides the Brass, Copper and S textures which are exhibited in the two kinds of as-rolled sheets, there are also Q and P texture components in the as-rolled CT sheets. The constitutive equation basing on evolution of dislocation mean free path (L) and dislocation cell size (d_{DC}) with plastic strain indicates that the initial values of L, d_{DC} and mobile dislocation density (ρ_m) are associated with annealing condition closely. Furthermore, the strain ranges of the stable and instable plastic deformation are related to the degree of recovery and recrystallization.

Keywords Roll · Anneal · Texture · Plastic · Dislocation cell

1 Introduction

There is a significant interest in the development of severe plastic deformation (SPD) methods, such as cold rolling, equal-channel angular pressing and high-pressure torsion, for obtaining ultrafine grain structures [1, 2]. The grain-refinement should be related to the high dislocation storage rate and low rate dynamic recovery [2]. Therefore, it is believed that cryogenically deformation enhances the refinement of grain size because the cryogenic temperature can suppress the dynamic recovery process and contribute to the increase of the dislocation density [3–5]. However, materials prepared by SPD often possess high strength but suffer from poor ductility due to the low dislocation accumulation capacity [1, 2]. In order to improve the ductility, the SPD materials are treated at low temperature generally, which can promote formation of the multi-length scale structures [4, 5].

However, due to the difference of dislocation density evolution in the different deformation ambient conditions, the texture evolution is distinct in the annealing process. Lapeire et al. [3] indicate that besides the texture difference between the RT and CT copper under deformation state, a very weak texture will be obtained after recrystallization process of CT Cu, which is contrast to the strong cube texture of RT Cu after recrystallization. Generally, the texture evolution in the annealing process is associated with the stability of the deformation texture. Due to the high vacancy content and low activation energy, the material produced by SPD at cryogenic temperature will access recrystallization at relatively low temperature [6, 7]. Even if the annealing temperature close to room temperature, the recrystallization microstructure may be observed in cryogenically rolled copper [6].

In addition, mechanical properties are related to the evolution of dislocation configuration such as dislocation cell (DC) and dense dislocation walls [8–10]. Then, the difference of plastic flow stress between RT and CT samples can be explained by the development of dislocation cell with the change of annealing condition or plastic strain [11]. Therefore, the effects of annealing process on the microstructure evolution of the RT and CT Cu–3 wt%Ag–0.5 wt%Zr thin sheets are studied in the present study. Furthermore, the

---

✉ Gang Chen
  cg@hitwh.edu.cn

1 School of Materials Science and Engineering, Harbin Institute of Technology at Weihai, 2 Wenhuaxi Road, Weihai 264209, China

dependencies of the tensile plastic deformation behaviours on the annealing microstructures are investigated to compare the differences of the mechanical properties of RT and CT samples. The reason for employing Cu–3 wt%Ag–0.5 wt%Zr as research material is that this alloy was widely used in the thrust chambers of rocket engines and space shuttle engines due to their excellent strength and thermal conductivity [12, 13].

2 Experimental Procedure

For homogenizing the texture of the Cu–3 wt%Ag–0.5 wt%Zr obtained by melting and cast method, the forging process is used to transform the as-cast rod to disk shape at the temperature between 800 and 850 °C. Many plates with thickness of 2 mm cutted from disk are annealed at 940 °C for 120 min for homogenizing components and softening the alloy. Then, the plates are thinned to 0.40 mm (corresponding to $\varepsilon_{vM} = 1.86$) by rolling process which are conducted at room temperature and cryogenic temperature produced by liquid nitrogen, respectively. The as-rolled samples are annealed at different temperature (200, 300, 400, 450, 500 and 600 °C) in an inert atmosphere for 1.0 h.

The Vickers microhardness (HV) measurements are performed on samples using a microhardness tester with a load of 2.94 N and dwell time of 15 s. All samples for the EBSD analysis are prepared by electro-polishing using a solution of 25% ethanol + 25% phosphoric + 50% distilled water. The orientation distribution function (ODF) sections with $\varphi_2 = 0°$, 45° and 65° are presented for characterizing the typical texture components. For TEM analysis some samples were punched into a 3 mm disk and polished into a thin foil with a thickness of 50–70 μm. Finally, ion milling was performed at 3–5 keV with continuous cooling of the sample by liquid nitrogen. Tensile test samples with gauge dimensions of 0.4 mm × 3 mm × 12 mm were machined from the as-rolled sheets parallel to the rolling direction. After being annealed for 60 min at different temperature, the samples are tensiled at room temperature by an INSTRON testing machine with a constant loading rate of 3.6 mm/min.

3 Results and Discussion

3.1 Microstructure and Texture Analysis

EBSD maps shown in Fig. 1 describe the recovery and recrystallization of the as-rolled RT sample. The cell block and lots of low angle boundaries (LABs) can be found in Fig. 1a, which verified the texture analysis results of the previous studies [3, 14]. After being treated at 200–400 °C, many lamellar structures rounded with high angle boundaries (HABs) and presented in the samples shown in Fig. 1b–d. Due to the occurrence of the recovery process, a large proportion of the cell and lamellar structure disappeared at temperature higher than 400 °C (Fig. 1d). As the temperature reaching to 450 °C, the equiaxed structure shown in Fig. 1e is the remarkable feature texture of the sample, which reveals the material undergo the initial stage of the recrystallization [15]. With the content of equiaxed structure increasing, the samples annealed at 500 °C consist of the coarse grain and a partially recovered texture which is described as bimodal microstructure (Fig. 1f). The microstructure of sample annealed at 600 °C is a coarse grain with few LABs (Fig. 1g), which suggests the very high recrystallization degree. Figure 1h shows the variation of the fraction of boundaries with different mis-orientation angles as the annealing temperature increases. The content of LABs and HABs change quickly as temperature higher than 500 °C, which indicates the high recrystallization degree of RT as-rolled sample heated at 500–600 °C for 1 h. Figure 2a illustrates the texture of as-rolled CT sample also consists of lamellar structures, cell block and LABs. The lamellar structures almost disappear at 200 °C, which suggests that the lamellar structure boundary (i.e. dense dislocation wall and microband) are more unstable than that in RT samples. From Fig. 2b–d, it can be found that with annealing temperature increasing, the proportion of sub-grain and cell block enclosed by HABs increases. As shown in Fig. 2d, many coarse equiaxed grains with diameter about 2–5 μm present in CT sample, which indicates that the recrystallization occurs at the temperature below 400 °C. As temperature increasing (Fig. 2f, g), the content of HAB and size of grain increase. Figure 2h illustrates that the fraction of LAB drops quickly as temperature higher than 450 °C, which indicates the CT as-rolled sample is easier to recrystallize than RT sample.

The textures are represented by orientation distribution functions (ODFs) and the results are described by Figs. 3 and 4. The main ideal orientations of face-centered cube (FCC) metal are shown in Fig. 3a. The texture of copper sheet rolled with reduction higher than 70% expresses as Copper type which contains Copper, Brass and S components [3, 4, 16–18]. Some alloy elements can decrease the stacking fault energy (SFE) of Cu substantially [19, 20]. Then, the texture converts into Brass-type rolling texture which is characterized by Brass and Goss components [17, 21]. Because Ag and Zr can reduce the SFE of Cu [5, 17, 19], the main texture of as-rolled RT sample presents as Brass, Copper and S (Fig. 3b). After samples are treated at 450 °C for 1 h, the Goss, Q and P components appear in the texture (Fig. 3c). The Goss type texture is generally associated with recrystallization or development of α-fiber which including Brass and Goss components [4, 18]. Figure 3d illustrates the maximum intensity of every texture

Fig. 1 The EBSD maps of the **RT** samples: **a** as-rolled; **b** 200 °C/1 h; **c** 300 °C/1 h; **d** 400 °C/1 h; **e** 450 °C/1 h; **f** 500 °C/1 h; and **g** 600 °C/1 h. **h** The fraction of boundaries with different misorientation angles
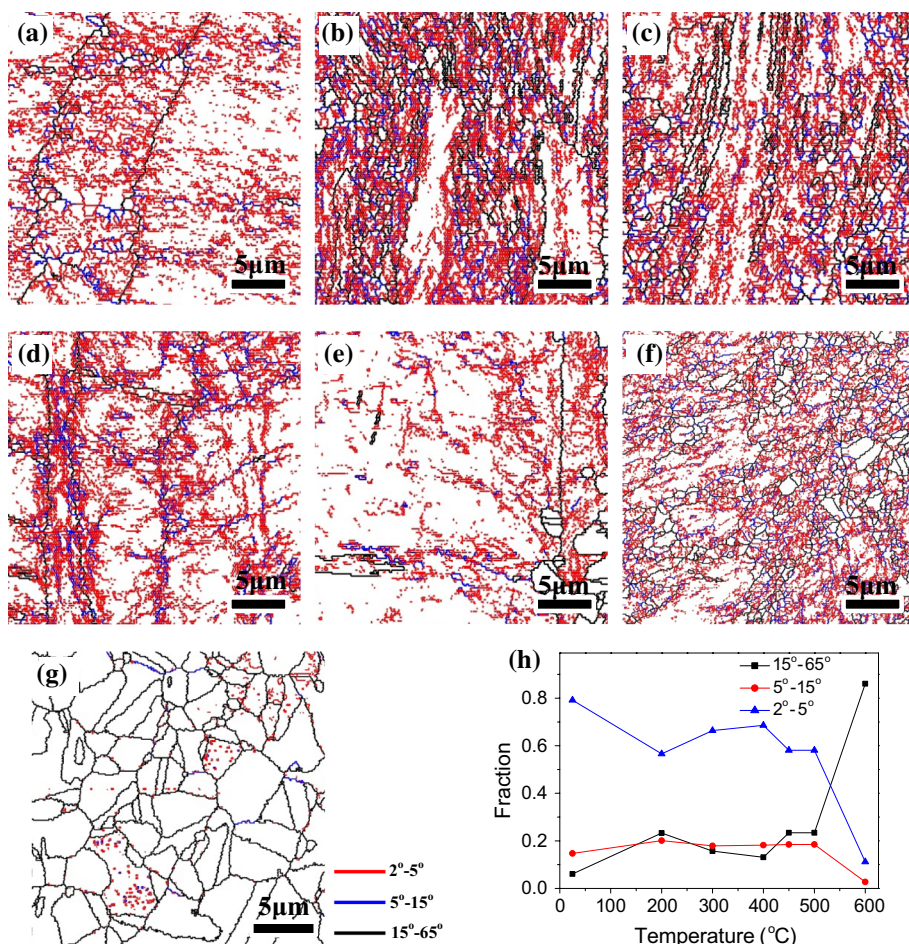
components reduces to the value lower than $10 \times$ random, which suggests the presenting of recrystallization texture in the sample treated at 500 °C. When the annealing temperature reaches to 600 °C, the textures corresponding to the ideal main orientations of FCC metal disappears in the samples. Therefore, the microstructure of recrystallization can be obtained for as-rolled RT sample annealed at 600 °C for 1 h. For as-rolled CT sample, the texture shown in Fig. 4b exhibits similar feature as the as-rolled RT sample. However, the Q and P components are most intense in Fig. 4b, which may be caused by the occurrence of recovery and recrystallization to some extent [3]. When annealing temperature is higher than 400 °C, the intensities of texture components are obviously weaken, which reveals the occurrence of the recrystallization process (Fig. 4c–e).

The Vickers microhardness curves of samples are shown in Fig. 5. It is speculated that the initial recrystallization temperature of RT sample is in the range of 400 to 450 °C (Fig. 5a), which is consistent with the analysis of microstructure. Because the reinforcement of precipitation will weaken the decrease of hardness caused by recrystallization, the initial recrystallization temperature of CT sample determined by microhardness curve (Fig. 5b) is in the

range of 300–400 °C which is higher than that described in Fig. 2. The recrystallization degree X can be calculated by the relation shown as Eq. 1 [22].

$$X = \frac{H_{max} - H_i}{H_{max} - H_{min}} \times 100\% \tag{1}$$

where H_{max} is the maximum hardness, H_i is the hardness for the given temperature, and H_{min} is the minimum hardness. The X value of RT sample being treated at 450 °C is about 29%. For CT sample being annealed at 400 °C, the X value reaches to ~ 18%.

The previous studies indicate that microstructure of as-rolled FCC sample shown in TEM images contains lots of parallel dense dislocation walls (DDWs), microband and a few cell blocks formed by extended dislocation boundaries [23–25]. Figure 6a shows that the texture of as-rolled RT sample occupies these microstructure characteristic. Figure 6b shows that the DDW regions contain parallel dislocation arrays which is also observed in typical pure fcc metals with large plastic deformation [25, 26]. As shown in Fig. 6c, some parallel DDWs disappear during the recovery of the sample annealed at 200° C for 1 h.

Fig. 2 The EBSD maps of
the CT samples: **a** as-rolled;
b 200 °C/1 h; **c** 300 °C/1 h;
d 400 °C/1 h; **e** 450 °C/1 h; **f**
500 °C/1 h; and **f** 600 °C/1 h. **h**
The fraction of boundaries with
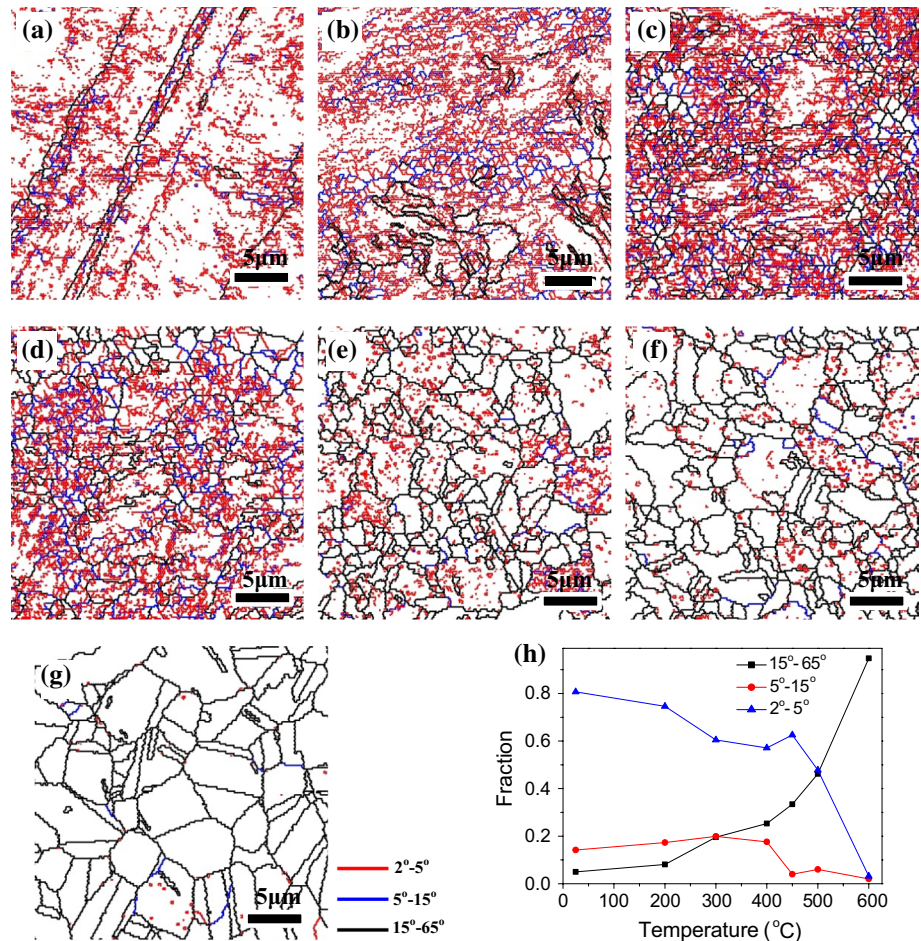different misorientation angles

Figure 6d, e illustrate that the microstructure of as-rolled CT sample is similar with that of as-rolled RT sample. Because the lower deformation temperature can reduce the dynamic recovery rate and promote the storage of dislocations in grain interior [27], the average size of cell structure is smaller than that shown in Fig. 6a, b. Besides the decrease of DDW density (Fig. 6f), the Ag precipitates can be found in the sample annealed at 200 °C for 1 h (Fig. 6g, h). Since the cube-on-cube orientation relationship between Ag precipitate and Cu matrix is easy to form [28, 29], the interface should present as semi-coherent mode generally. Due to the lattice mismatch between the Cu and Ag crystals, atoms across the interface are distinguished into three types of lattice sites including the FCC region, misfit dislocation region and misfit dislocation intersections (nodes) corresponding to a relative rotation and dilation/compression regions between two crystals [29]. Figure 6h shows that the nodes labeled by red circles arrange regularly and periodically. The fast Fourier transform (FFT) image in Fig. 6h illustrates that the interface is perpendicular to the direction of observation and parallel to {110} of Cu and Ag crystals. Then, the indexes of crystal faces are determined and labeled by solid red

lines in Fig. 6h. These precipitations can pin the dislocation, which will promote the elevation of material strength [30–32]. Straumal et al. [33] suggested that the formation of Ag-base phase precipitates at low annealing temperature relates to the unstability of supersaturated solid solution under SPD at cryogenic condition.

3.2 Tensile Deformation Behaviours

Generally, the flow stress (σ) can be expressed by Eq. 2.

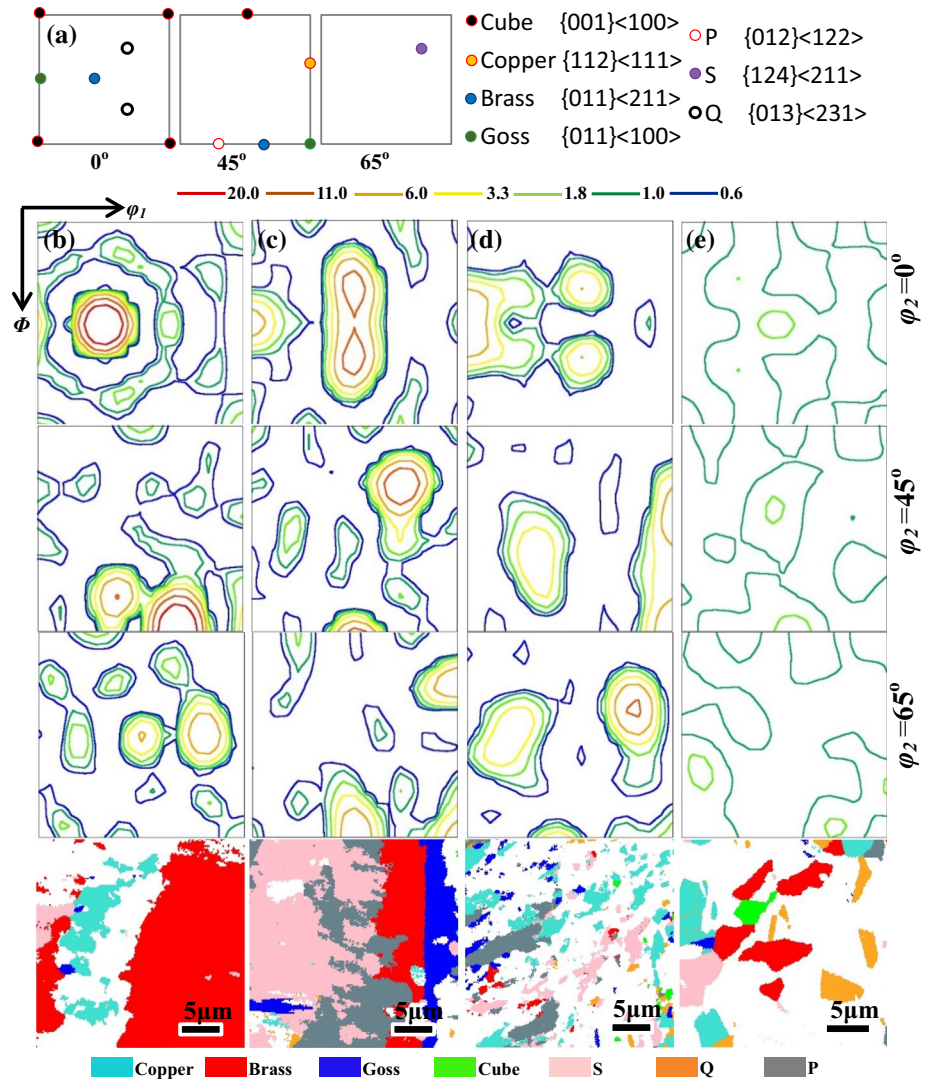$$\sigma = M \cdot \alpha \cdot \mu \cdot b \cdot \sqrt{\rho} \tag{2}$$

where ρ is the total dislocation density, α is a constant, μ is the shear modulus of matrix, b is the matrix Burgers vector, and M is the Taylor factor [34].

Verier [35] and Kubin et al. [36] suggest that the mean free path (L) of movable dislocations is inversely proportional to stress in each slip system. Then, the relationship between ρ and L can be expressed as Eq. 3.

$$\sqrt{\rho} = k/L \tag{3}$$

Keller et al. [37] indicate that the evolution of L in the plastic deformation process can be described by Eq. 4.

Fig. 3 The ODF sections ($\varphi_2 = 0°, 45°, 65°$) and EBSD maps of the texture components (within 15° tolerance) of RT samples: **a** main ideal orientations existing in rolled fcc material; **b** as-rolled; **c** 450 °C/1 h; **d** 500 °C/1 h; **e** 600 °C/1 h

Because the size of dislocation cellular structures is known to scale with $\rho^{-0.5}$ [10], the flow stress can be described by Eq. 8.

$$\sigma = M \cdot \alpha \cdot \mu \cdot b \cdot k_2 / d_{DC} \tag{8}$$

where, the k_2 is in the range of 10–20 [10, 39, 40], and for copper $k_2 \approx 16$ [39].

By combining the Eqs. 7 and 8, the σ–ε curves of RT and CT samples could thus be calculated and shown in Fig. 7. The evolution of d_{DC} in the plastic deformation process can also be obtained and describe by Fig. 8. The results indicate that the features of samples with different degree of recovery and recrystallization is closely related to the d_{DC} values.

The strain dependence of mobile (ρ_m) and immobile (ρ_f) dislocation density, namely classic KE model [41, 42], described as Eqs. 9 and 10 are used to calculate L_y and L_s.

$$\frac{d\rho_m}{d\varepsilon} = C_1 - C_2 \cdot \rho_m - C_3 \cdot (\rho_f)^{1/2} \tag{9}$$

$$\frac{dL}{d\varepsilon} = -k_L \cdot (L - L_s) \tag{4}$$

where, the k_L is the parameter describing the rate of evolution of L and L_s is the saturation value of L. The initial value (L_y) of L relates to the onset of deformation. Then, Eq. 4 can be integrated as follow:

$$\frac{L - L_s}{L_y - L_s} = \exp(-k_L \cdot \varepsilon) \tag{5}$$

$$L = (L_y - L_s) \cdot \exp(-k_L \cdot \varepsilon) + L_s \tag{6}$$

The previous studies suggest that there are linear relationship between d_{DC} and L [38, 39]. Therefore, the d_{DC} can be expressed as Eq. 7 by introducing adjustable parameter (k_3 and k_4).

$$d_{DC} = k_3 \cdot [(L_y - L_s) \cdot \exp(-k_L \cdot \varepsilon) + L_s] + k_4 \tag{7}$$

Fig. 4 The ODF sections ($\varphi_2 = 0°$, 45°, 65°) and EBSD maps of the texture components (within 15° tolerance) of **CT** samples: **a** main ideal orientations existing in rolled fcc material; **b** as-rolled; **c** 400 °C/1 h; **d** 450 °C/1 h; **e** 500 °C/1 h
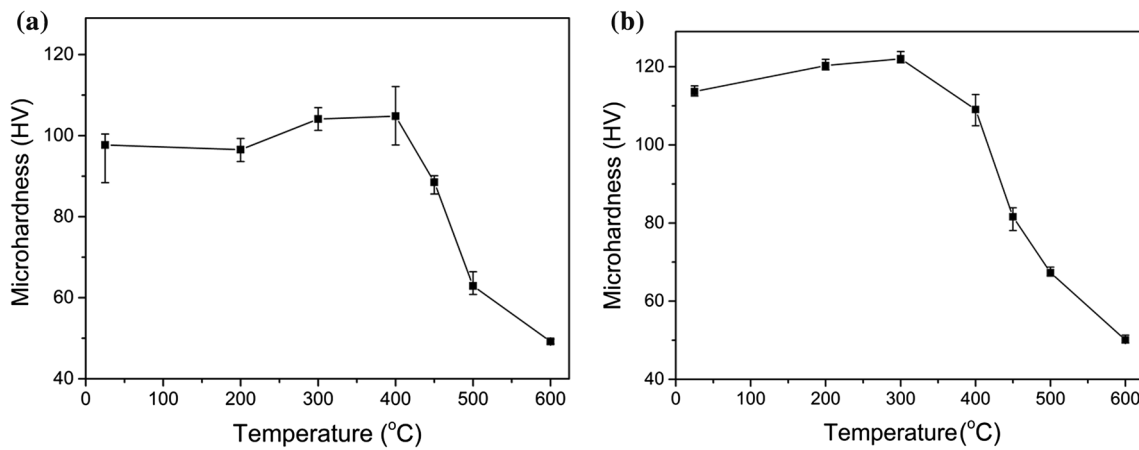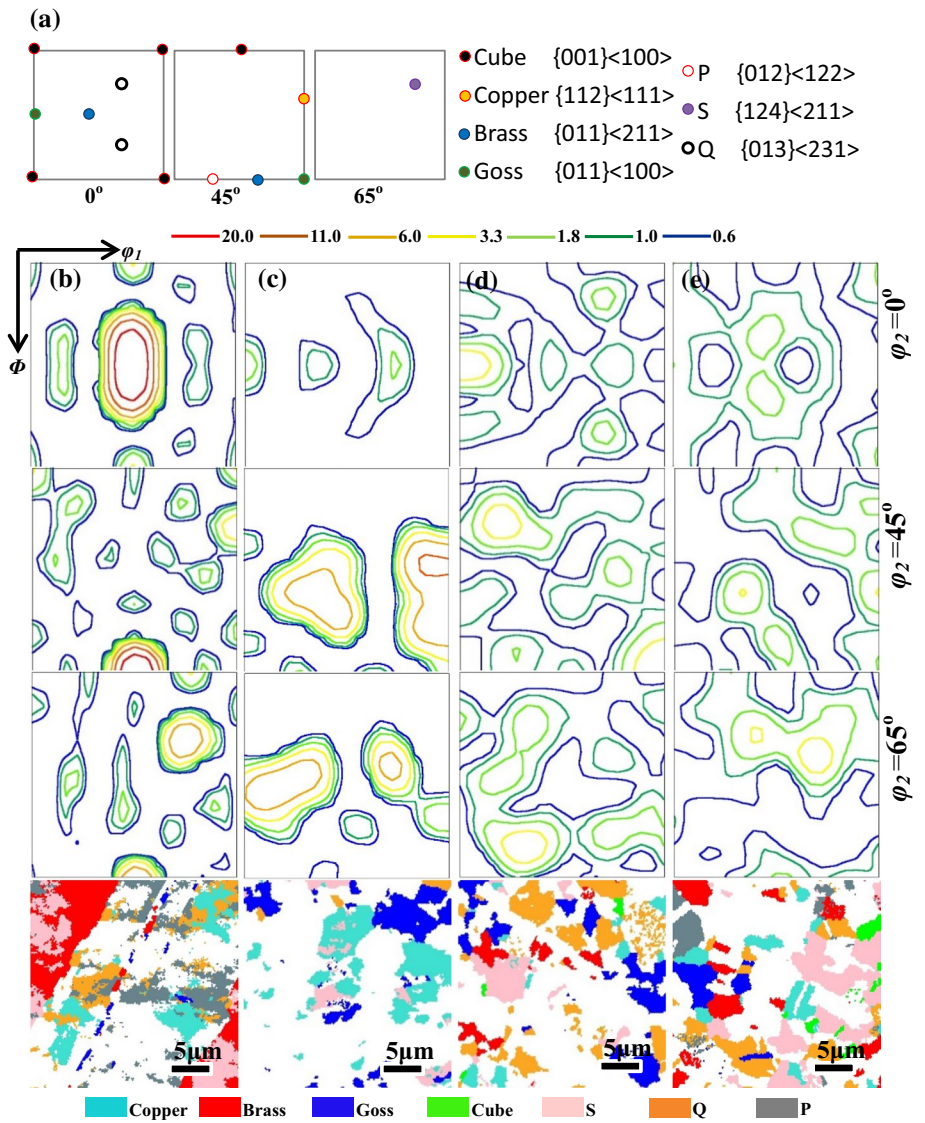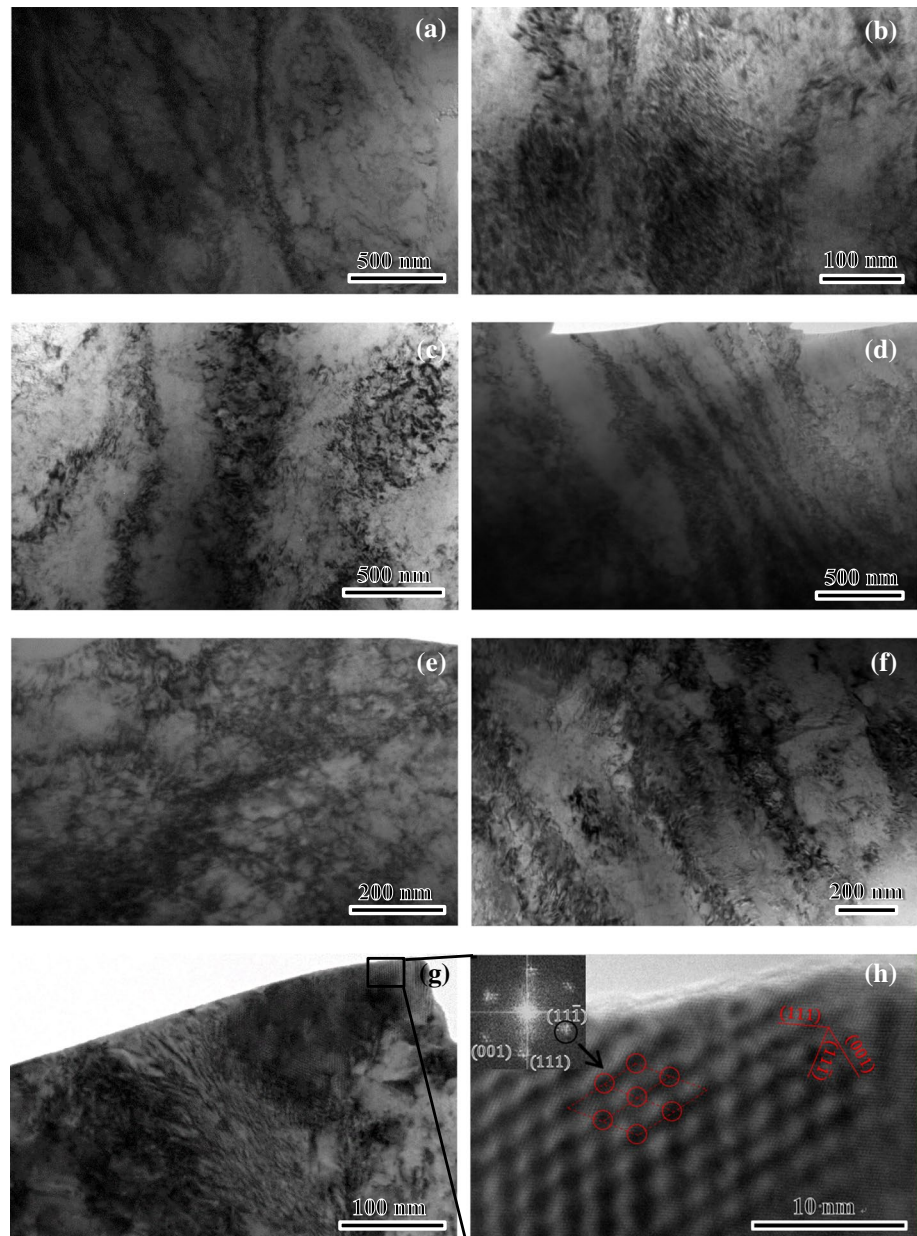

Fig. 5 The HV value as a function of annealing temperature of Cu–3 wt%Ag–0.5 wt%Zr alloy: **a** RT sample; **b** CT sample

Fig. 6 TEM images: **a**, **b** as-rolled RT sample; **c** RT 200 °C/1 h; **d**, **e** as-rolled CT sample; **f–h** CT 200 °C/1 h

$$\frac{d\rho_f}{d\varepsilon} = C_2 \cdot \rho_m + C_3 \cdot (\rho_f)^{1/2} - C_4 \cdot \rho_f \tag{10}$$

Because the ρ is the sum of ρ_m and ρ_f, one eventually obtains:

$$\frac{d\rho}{d\varepsilon} = C_1 - C_4 \cdot \rho_f \tag{11}$$

$$\frac{d^2\rho}{d\varepsilon^2} = -C_4 \cdot \left(\frac{d\rho}{d\varepsilon} - \frac{d\rho_m}{d\varepsilon} \right) \tag{12}$$

Keller et al. [37] suggested the ρ_m relates with L and can be expressed as:

$$\frac{d\rho_m}{d\varepsilon} = \frac{M}{b} \cdot \left(\frac{1}{L_s} - \frac{1}{L} \right) \tag{13}$$

Taking into account the evolution of L, Eq. 13 changes into the following formation:

$$\frac{d\rho_m}{d\varepsilon} = \frac{M \cdot (L_y - L_s) \cdot \exp(-k_L \cdot \varepsilon)}{b \cdot [(L_y - L_s) \cdot \exp(-k_L \cdot \varepsilon) + L_s] \cdot L_s} \tag{14}$$

The ρ_m and L can be obtained and shown in Fig. 9 based on Eqs. 7, 8, 12 and 14. Generally, due to the elevation of the recovery and recrystallization degree, the initial ρ_m ($\varepsilon = 0$) decreases with the increase of annealing
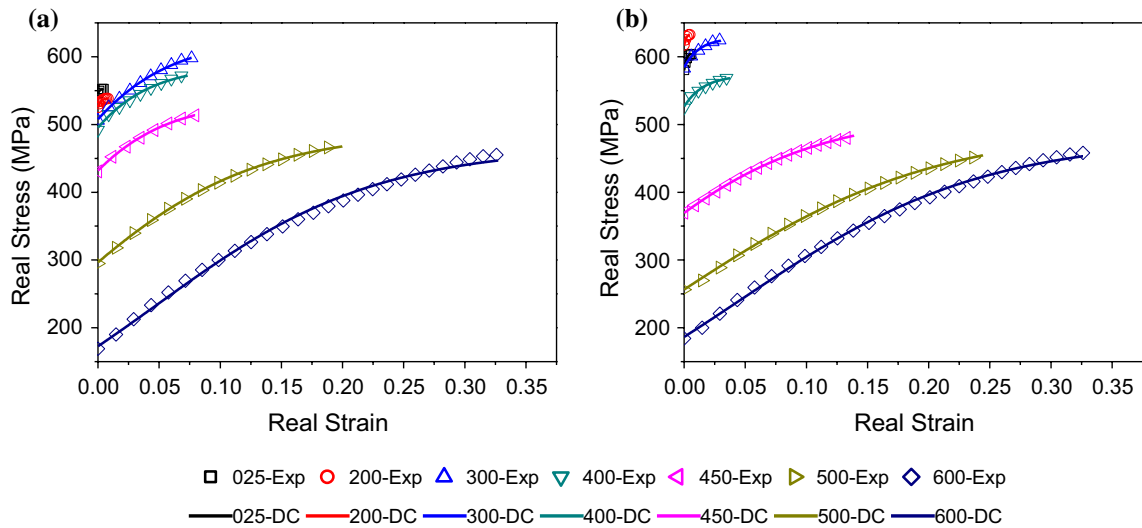
Fig. 7 The real stresse-strain curves of samples annealed at different temperatures: **a** RT samples; **b** CT samples
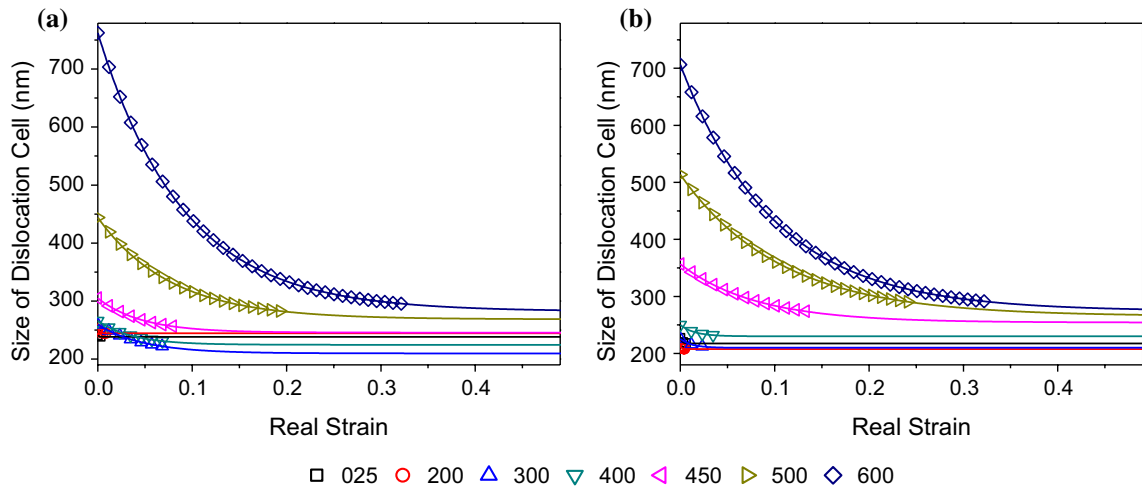

Fig. 8 The d_{Dc} versus ε curves: **a** RT samples; **b** CT samples

temperature, as seen in Fig. 10. Furthermore, along with the reduction of initial ρ_m, the original value of L and d_{DC} increases. It should be noted that the variation tendency of initial ρ_m, L and d_{DC} is effected by the Ag precipitation of the CT samples at temperature lower than 400 °C. Though the differences in initial values of ρ_m and dc are big, the values in their saturation state are similar to each other shown in Figs. 8, 9a, b. The saturation d_{DC} values of all samples are in the range of 200–300 nm. And Fig. 9a, b indicate that the saturation ρ_m values are in the range of $1–3 \times 10^{15}/m^2$. In the recovery process, the initial ρ_m, L and d_{DC} vary slightly, which is corresponding to the slight reduction of ρ in the sample. However, due to the effects

of recrystallization, these parameters will vary abruptly as the annealing temperature increasing.

The varying pattern of the necked strain (ε_{neck}) shown in Fig. 11 is similar to that of initial ρ_m, L and d_{DC}. That is to say, the range of strain in the stable plastic deformation stage increases obviously when the recrystallization happens in the annealing process. In addition, due to the elevation of the strain of the fractured sample ($\varepsilon_{fracture}$), the instable plastic deformation ($\varepsilon_{fracture} - \varepsilon_{neck}$) stage also increases with the annealing temperature increasing, which indicates the role of intervoid necking is weakened for the sample with recrystallization texture.
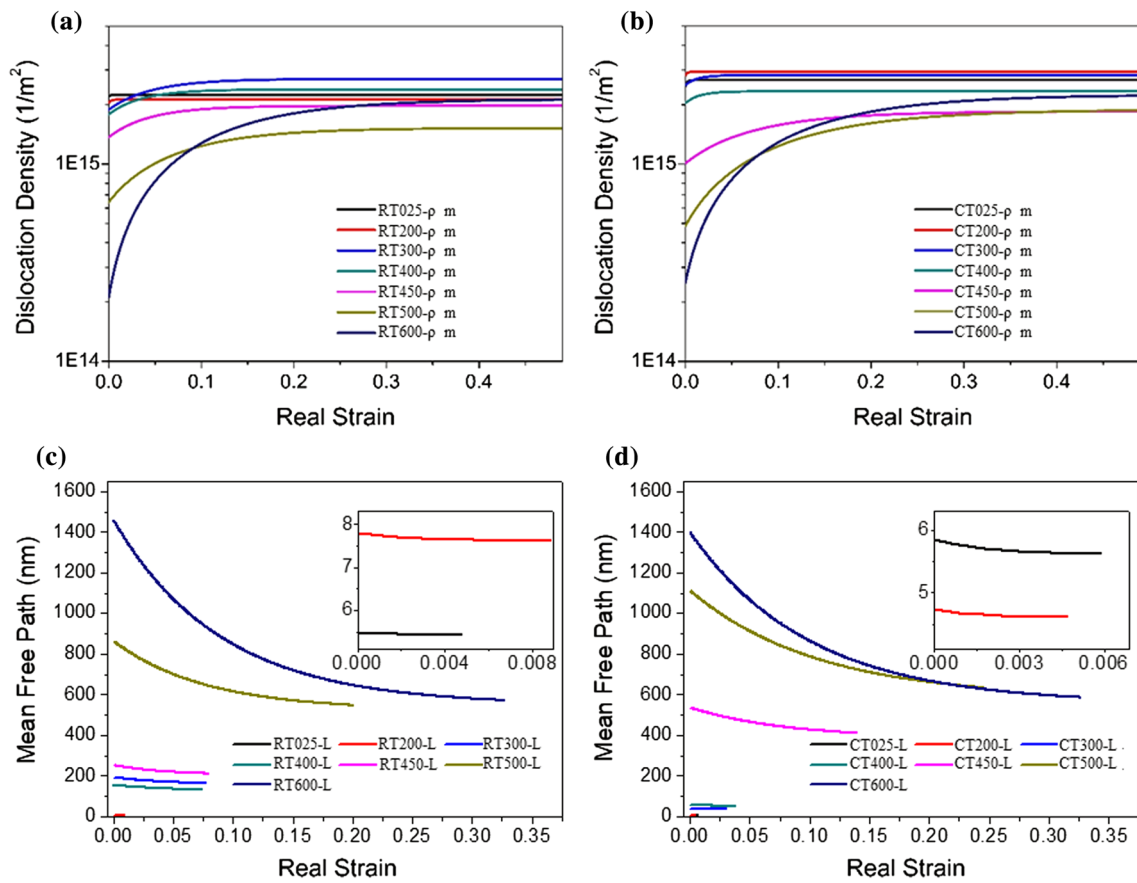
Fig. 9 The ρ_m versus ε curves of samples annealed at different temperatures: **a** RT samples; **b** CT samples; the L versus ε curves of samples: **c** RT samples; **d** CT samples
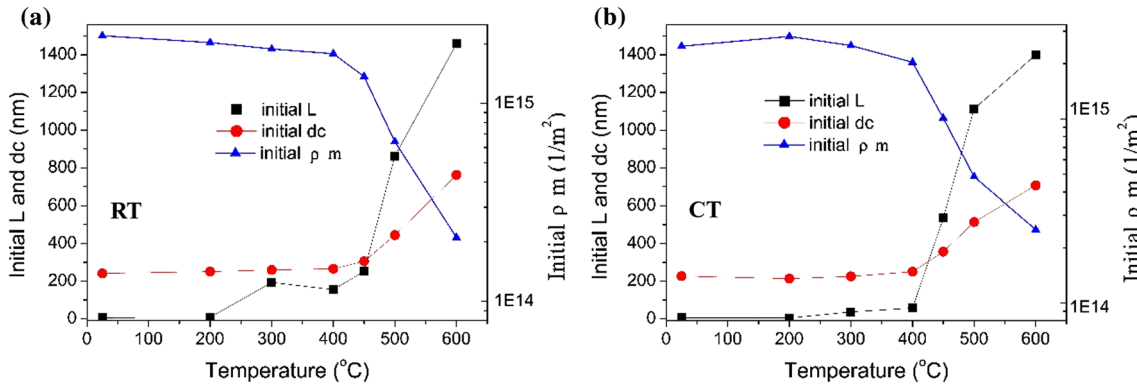

Fig. 10 The initial L and d_{Dc}: **a** RT samples; **b** CT samples

4 Conclusion

The effect of annealing process on the microstructure, texture evolutions and tensile plastic deformation of RT and CT Cu–3 wt%Ag–0.5 wt%Zr sheets are researched in the present study.

The heat stability of the as-rolled RT sample is better than that of CT sample, due to its recrystallization happening at higher temperature. The contents of LAB and HAB change quickly when recrystallization presents in the samples. The main texture components of as-rolled RT and CT samples comprise Brass, Copper and S textures. However, there are also Q and P textures in the as-rolled CT sheets. The
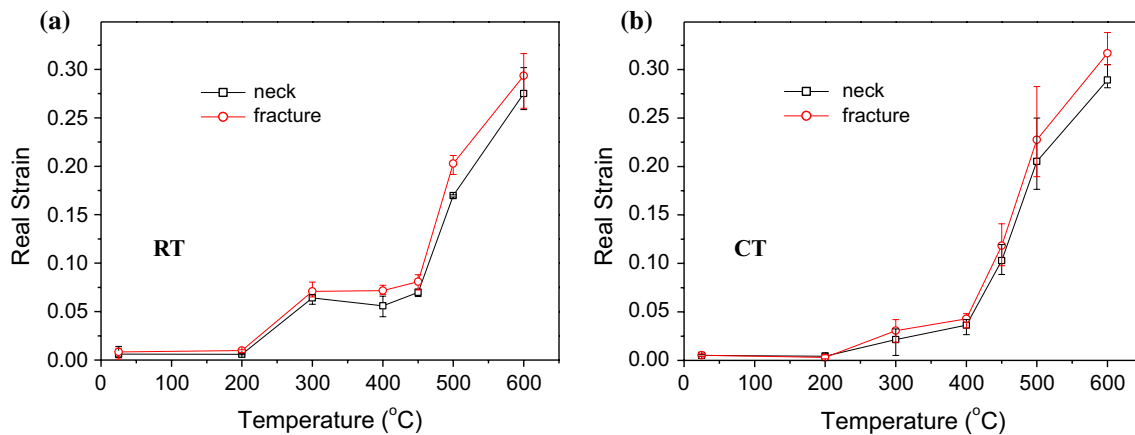
Fig. 11 The neck and fracture strain: **a** RT samples; **b** CT samples

maximum intensity of texture components shown in ODF picture reduces obviously as the occurrence of recrystallization. For as-rolled CT sample annealed at 200 °C, there are Ag precipitates separating from matrix and forming the typical semi-coherent interface structure between Cu and Ag.

The tensile plastic deformation can be described by constitutive model considering the evolution of d_{DC} or L. Due to the elimination of dislocation in the recovery and recrystallization process, the initial values of L, d_{DC} and ρ_m vary with the annealing temperature. For the sample with high degree recovery and recrystallization, its instable plastic deformation stage is longer than that of as-rolled sample.

References

1. A. Vinogradov, Y. Estrin, Analytical and numerical approaches to modelling severe plastic deformation. Prog. Mater. Sci. **95**, 172–242 (2018)

2. G. Faraji, H.S. Kim, H.T. Kashi, *Severe Plastic Deformation Methods, Processing and Properties* (Elsevier, Amsterdam, 2018). https://doi.org/10.1016/C2016-0-05256-7

3. L. Lapeire, J. Sidor, P. Verleysen, K. Verbeken, I. De Graeve, H. Terryn, L.A.I. Kestens, Texture comparison between room temperature rolled and cryogenically rolled pure copper. Acta Mater. **95**, 224–235 (2015)

4. T. Konkova, S. Mironov, A. Korznikov, M.M. Myshlyaev, S.L. Semiatin, Annealing behavior of cryogenically-rolled copper. Mat. Sci. Eng. A **585**, 178–189 (2013)

5. Y. Lu, R. Ma, Y.N. Wang, Texture evolution and recrystallization behaviors of Cu–Ag alloys subjected to cryogenic rolling. Trans. Nonferrous Met. Soc. China **25**, 2948–2957 (2015)

6. T. Konkova, S. Mironov, A. Korznikov, S.L. Semiatin, Microstructure instability in cryogenically deformed copper. Scr. Mater. **63**, 921–924 (2010)

7. C. Saldana, A.H. King, S. Chandrasekar, Thermal stability and strength of deformation microstructures. Acta Mater. **60**, 4107–4116 (2012)

8. D.A. Hughes, N. Hansen, The microstructural origin of work hardening stages. Acta Mater. **148**, 374–383 (2018)

9. M.N. Bassim, C.D. Liu, Dislocation cell structures in copper in torsion and tension. Mater. Sci. Eng. A **164**, 170–174 (1993)

10. E.I. Galindo-Nava, P.E.J. Rivera-Díaz-del-Castillo, A thermodynamic theory for dislocation cell formation and misorientation in metals. Acta Mater. **60**, 4370–4378 (2012)

11. G. Chen, J.Z. Shen, Q. Zhu, S.J. Yao, C.J. Wang, P. Zhang, Tensile deformation and fracture behaviours of cold rolled Cu–3wt.%Ag–0.5wt.%Zr thin sheets with different annealed microstructures. Mater. Sci. Eng. A **756**, 27–34 (2019)

12. P.S. Chen, J.H. Sanders, Y.K. Liaw et al., Ductility degradation of vacuum-plasma-sprayed NARloy-Z at elevated temperatures. Mater. Sci. Eng. A **199**(2), 145–152 (1995)

13. C. Verdy, *Ipsé—LERMPS*. Phd thesis, Belfort, France, 1998, 279 pp

14. N. Hansen, X. Huang, D.A. Hughes, Microstructural evolution and hardening parameters. Mater. Sci. Eng. A **317**, 3–11 (2001)

15. T.B. Yu, N. Hansen, X.X. Huang, Linking recovery and recrystallization through triple junction motion in aluminum cold rolled to a large strain. Acta Mater. **61**, 6577–6586 (2013)

16. D.K. Wilsdorf, N. Hansen, Geometrically necessary, incidental and subgrain boundaries. Scr. Metall. Mater. **25**, 1557–1562 (1991)

17. R.G. Li, S.J. Zhang, H.J. Kang, Z.N. Chen, F.F. Yang, W. Wang, C.L. Zou, T.J. Li, T.M. Wang, Microstructure and texture evolution in the cryorolled CuZr alloy. J. Alloys. Compd. **693**, 592–600 (2017)

18. T. Konkova, S. Mironov, A. Korznikov, S.L. Semiatin, Microstructural response of pure copper to cryogenic rolling. Acta Mater. **58**, 5262–5273 (2010)

19. Q.Q. Shao, L.H. Liu, T.W. Fan, D.W. Yuan, J.H. Chen, Effects of solute concentration on the stacking fault energy in copper alloys at finite temperatures. J. Alloys. Compd. **726**, 601–607 (2017)

20. B.B. Zhang, N.R. Tao, K. Lu, A high strength and high electrical conductivity bulk Cu–Ag alloy strengthened with nanotwins. Scr. Mater. **129**, 39–43 (2017)

21. T. Konkova, S. Mironova, A. Korznikov, G. Korznikova, M.M. Myshlyaev, S.L. Semiatin, An EBSD investigation of cryogenically-rolled Cu–30%Zn Brass. Mater. Charact. **101**, 173–179 (2015)

22. K.S. Raju, V.S. Sarma, A. Kauffmann, Z. Hegedűs, J. Gubicza, M. Peterlechner, J. Freudenberger, G. Wilde, High strength and ductile ultrafine-grained Cu–Ag alloy through bimodal grain size, dislocation density and solute distribution. Acta Mater. **61**(1), 228–238 (2013)

23. Z.P. Luo, H.W. Zhang, N. Hansen, K. Lu, Quantification of the microstructures of high purity nickel subjected to dynamic plastic deformation. Acta Mater. **60**, 1322–1333 (2012)

24. P. Landau, R.Z. Shneck, G. Makov, A. Venkert, Microstructure evolution in deformed copper. J. Mater. Sci. **42**, 9775–9782 (2007)

25. P. Landau, G. Makov, R.Z. Shneck, A. Venkert, Universal strain–temperature dependence of dislocation structure evolution in face-centered-cubic metals. Acta Mater. **59**, 5342–5350 (2011)

26. J. Gan, J.S. Vetrano, M.A. Khaleel, Microstructure characterization of dislocation wall structure in aluminum using transmission electron microscopy. J. Mater. Sci. Technol. **124**, 297–301 (2002)

27. C.Y. Yu, P.W. Kao, C.P. Chang, Transition of tensile deformation behaviors in ultrafine-grained aluminum. Acta Mater. **53**, 4019–4028 (2005)

28. W. Piyawit, W.Z. Xu, S.N. Mathaudhu, J. Freudenberger, J.M. Rigsbee, Y.T. Zhu, Nucleation and growth mechanism of Ag precipitates in a CuAgZr alloy. Mater. Sci. Eng. A **610**, 85–90 (2014)

29. S. Shao, J. Wang, A. Misra, Energy minimization mechanisms of semi-coherent interfaces. J. Appl. Phys. **116**, 023508(1–10) (2014)

30. J.B. Liu, M.L. Hou, H.Y. Yang, H.B. Xie, C. Yang, J.D. Zhang, Q. Feng, L.T. Wang, L. Meng, H.T. Wang, In-situ TEM study of the dynamic interactions between dislocations and precipitates in a Cu–Cr–Zr alloy. J. Alloys. Compd. **765**, 560–568 (2018)

31. H.D. Fu, S. Xu, W. Li, J.X. Xie, H.B. Zhao, Z.J. Pan, Effect of rolling and aging processes on microstructure and properties of Cu–Cr–Zr alloy. Mater. Sci. Eng. A **700**, 107–115 (2017)

32. J. Gubicza, Z. Hegedűs, J.L. Lábár, A. Kauffmann, J. Freudenberger, V.S. Sarma, Solute redistribution during annealing of a cold rolled Cu–Ag alloy. J. Alloys. Compd. **623**, 96–103 (2015)

33. B.B. Straumal, A.R. Kilmametov, A. Korneva, A.A. Mazilkin, P.B. Straumal, P. Zieba, B. Baretzky, Phase transitions in Cu-based alloys under high pressure torsion. J. Alloys. Compd. **707**, 20–26 (2017)

34. U.F. Kocks, H. Mecking, Physics and phenomenology of strain hardening: the FCC case. Prog. Mater Sci. **48**, 171–273 (2003)

35. R. Verier, Dislocation mean free path in copper at 77 K. Scr. Metall. **12**, 69–73 (1978)

36. B. Devincre, T. Hoc, L. Kubin, Dislocation mean free paths and strain hardening of crystals. Science **320**, 1745–1748 (2008)

37. C. Keller, E. Hug, Kocks–Mecking analysis of the size effects on the mechanical behavior of nickel polycrystals. Int. J. Plasticity **98**, 106–122 (2017)

38. A.W. Thompson, M.I. Baskes, W.F. Flanagan, The dependence of polycrystal work hardening on grain size. Acta Metall. **21**, 1017–1028 (1973)

39. A. Molinari, G. Ravichandran, Constitutive modeling of high-strain-rate deformation in metals based on the evolution of an effective microstructural length. Mech. Mater. **37**, 737–752 (2005)

40. D. Kuhlmann-Wilsdorf, Theory of plastic deformation: properties of low energy dislocation structures. Mater. Sci. Eng. A **113**, 1–41 (1989)

41. L.P. Kubin, Y. Estrin, Evolution of dislocation densities and the critical conditions for the portevin-le châtelier effect. Acta Metall. Mater. **38**, 697–708 (1990)

42. N.Q. Chinh, T. Csanádi, J. Gubicza, T.G. Langdon, Plastic behavior of face-centered-cubic metals over a wide range of strain. Acta Mater. **58**, 5015–5021 (2010)